Infante-García, D.; Zabala, A.; Giner Maravilla, E.; Llavori, I. (2022). On the use of the theory of critical distances with mesh control for fretting fatigue life assessment in complete and nearly complete contacts. Theoretical and Applied Fracture Mechanics. 121:1-12. https://doi.org/10.1016/j.tafmec.2022.103476

On the use of the theory of critical distances with mesh control for fretting fatigue life assessment in complete and nearly complete contacts.

D. Infante-Garcia[1], A. Zabala[2], E. Giner[1], I. Llavori[2]

[1]*Institute of Mechanical and Biomechanical Engineering - I2MB, Dpt. of Mechanical Engineering and Materials, Universitat Politècnica de València, Camino de Vera s/n, 46022 Valencia, Spain*

[2]*Mondragon Unibertsitatea, Faculty of Engineering, Mechanics and Industrial Production, Loramendi 4, Mondragon 20500, Gipuzkoa, Spain*

*Corresponding author: D. Infante-García (dieingar@upvnet.upv.es)

ABSTRACT.

In this work, the theory of critical distances using point method and mesh control approach for fretting fatigue life prediction in complete and nearly complete contacts is analysed. The approach is applied to thirty experimental tests found in the literature, where almost nine hundred simulations are carried out. The work concludes that the theory of critical distances using mesh control is able to predict the fretting fatigue strength of components using an optimum mesh size of 1.6 times the critical distance for all contact configurations analysed. Due to the use of an element size of around the critical distance length, the computational cost can be reduced up to 98% in comparison with the traditional theory of critical distances.

KEYWORDS. Fretting fatigue, Theory of Critical Distances (TCD), Multiaxial fatigue, Mesh control

1. Introduction

Fretting fatigue involves cyclic fluctuating stress and strains in solids in contact under relative tangential displacement [1]. The main fretting fatigue consequence is the rapid initiation and growth of cracks, although other surface damage mechanisms arise such as wear or corrosion. Therefore, fretting fatigue may lead to the premature or catastrophic component failure [2].

In fretting problems, two main groups of contacts can be distinguished: complete and incomplete contacts. When the contact area is independent of the normal load, the contact is said to be complete. On the other hand, the extension of the contact depends on the deformation of the bodies for incomplete contacts [3]. Complete contacts or nearly complete contacts such as the contact between

a flat surface against a flat indenter with rounded edges are found in many mechanical components, e.g. dovetail or fir-tree joints of gas turbines.

Fretting fatigue prediction of life and strength has been particularly interested during the last decades to optimize mechanical designs while avoiding large experimental testing campaigns. Predictive models of fretting fatigue are usually similar to those applied in notched components [4] or at sharp stress raisers such as the 'crack-like' notch analogue methodology [5,6]. The main reason is because of the severe stress gradient found in fretting fatigue problems around the contact edges can be analogous to the stress gradients close to a notch or a crack tip. However, it is worth mentioning that other surface damage mechanisms (e.g. wear of the surfaces) are omitted when applying predictive approaches from notch components which may affect the fatigue response. Methodologies found in the literature are commonly based on the idea of averaging the stress field over a process volume around the hot-spot in order to consider the stress gradient [7–10] such as the theory of critical distances (TCD) [11]. Among the different criteria available in the TCD, the point method (PM) is the simplest one, which states that failure will happen when the stress range at a distance $L/2$ from the notch root is equal to σ_0, being L the so-called critical distance, and $\Delta\sigma_0$ the range of the fatigue limit. The value of L can be calculated using cyclic material constants as follows

$$L = \frac{1}{\pi}\left(\frac{\Delta K_{th}}{\Delta\sigma_0}\right)^2 \tag{1}$$

being ΔK_{th} the fatigue crack propagation threshold. Note that the range of the fatigue limit and the fatigue crack propagation threshold should be obtained using the same load ratio. Previous works have shown the validity of TCD to assess fretting fatigue lifetime [12–20].

The application of the approach usually requires finite element analysis (FEA) to obtain an approximation of the stress field, because closed form solutions in fretting fatigue problems are only available for a few problems where half-space assumptions can be taken. FEA of fretting problems may involve a high computational cost due to the extreme stress gradients around contact edges in fretted regions. The mesh sensitivity analysis usually reveals an element size of a few microns, limiting the analyses mainly to two-dimensional under transverse plane strain conditions. In order to avoid the use of very refined meshes, Vargiu et al. [21] proposed the TCD with mesh control (MC), which consists in to pre-set the element size d to a multiplier α of L in such a way that the hot-spot stress obtained with the coarse mesh is the same value as the one obtained with TCD point method with a refined mesh. The TCD with mesh control was originally applied to notched specimens. In addition, the authors of this work previously showed the viability of the TCD with mesh control

approach for fretting fatigue life prediction in incomplete contacts using the Smith-Watson-Topper model [8].

The present work extends the original analysis of the viability of using the TCD with mesh control approach to fretting fatigue life prediction in complete and nearly complete contacts. Three contact configurations are analysed: cylinder to flat contact, flat-to-flat with sharp edges contact and flat-to-flat with rounded edges. In this way, a parametric analysis with different synthetic critical distances is firstly performed to assess the optimum mesh size. Next, the validity of the selected optimum mesh size is evaluated in thirty experimental test conditions. The study includes a fretting fatigue problem using an incomplete contact as a reference from the previous study [8] to compare the differences in the results obtained with complete and nearly complete contacts.

2. Contact mechanics

Three contact configurations commonly used in fretting fatigue testing are reviewed in this section. The objective of this section is to summarize the main characteristics of the contact tractions, to highlight differences and similarities, and to give some historical background of each contact configuration. The three contact configurations are simplified to a specimen with a flat surface pressed into a pad or punch under normal constant load (see Fig. 1 and 2), namely: a cylindrical pad, a square-ended flat punch and a flat punch with rounded edges. It is noteworthy that several hypotheses are taken during the analytical development of the contact solutions presented above: (i) contact bodies behave as purely elastic solids with smooth surfaces, (ii) elastic-half space approximation, (iii) pad radius is significantly larger than contact length, and (iv) similar elastic properties of both solids in contact.

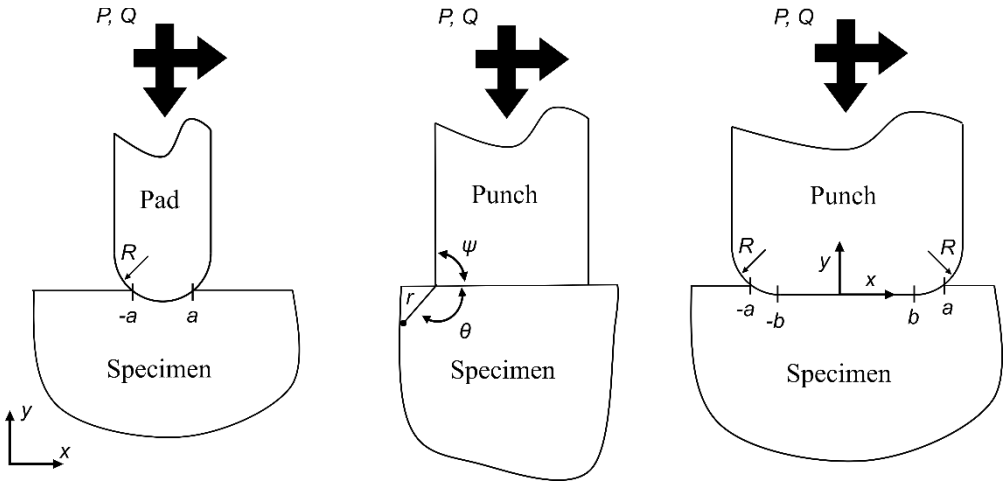

Fig. 1.: From left to right: Sketch of a cylinder pad pressed onto a flat surface, a square-ended punch pressed onto a flat surface and a flat punch with rounded edges to flat surface contact configuration.

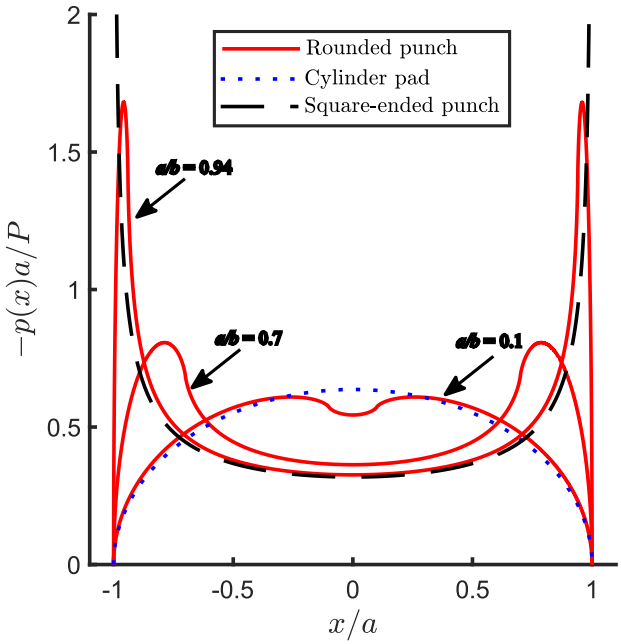

Fig. 2.: Normal pressure distribution for the cylinder pad, rounded punch, and square-ended punch pressed with different *a/b* ratios onto a flat surface.

2.1 Cylindrical pad to flat contact configuration (CTF)

The first solution of this type of contact belongs to the well-known Hertzian theory of non-conforming smooth curved surfaces in contact [22,23]. In this type of non-conforming contact, the initial contact area is a line and depends on the normal load *P*. One of the main characteristics of this contact configuration is that the contact pressure decreases to zero on the contact edges (see Eq. 1). The normalized distribution is shown in Fig. 2 (blue dotted line).

$$p(x) = -p_0\sqrt{1-\left(\frac{x}{a}\right)^2} \tag{1}$$

$$p_0 = \frac{2P}{\pi a} \tag{2}$$

$$a^2 = \frac{2PA}{\pi k} \tag{3}$$

being p_0 the peak contact pressure, a is the contact half-width, k is the relative curvature and $A = \left(\frac{1-\nu_1^2}{E_1} + \frac{1-\nu_2^2}{E_2}\right)$ is the composite compliance where E and ν are the elastic modulus and Poisson's ratio for each component in contact, respectively. Note that in this case the relative curvature is the radius

of the cylinder, and the composite compliance is usually calculated for transverse plane strain conditions in contact problems. The solution under tangential load *Q* was given by Cattaneo and Mindlin [24,25] and under superimposed cyclic axial load was obtained by Hills et al. [26]. These analytical solutions have been the basis for failure assessment in a multitude of fretting fatigue work [27].

2.2 Square-ended flat punch to flat contact configuration (FTFS)

Where two flat surfaces are brought into contact and fit exactly without deformation (see Fig. 1), the contact is said to be complete, such as when using squared-ended flat punches to a flat surface. In contrast to the previous contact configuration, in this case the contact area is independent of the normal load and the stress field at the contact edges is usually singular as shown in Fig. 2.

Under complete adhesion, the stress field surrounding the contact edge can be related to the stress field found in the corner of a single wedge, solution found by Williams [28]. The stress state under symmetric loading is defined to be of the form of Eq. 4.

$$\sigma_{ij}(r,\theta) = \frac{K_i}{r^{1-\lambda}} f_{ij}(\theta) \tag{4}$$

where $f_{ij}(\theta)$ are the angular eigenfunctions and *K* is the associated generalized stress intensity factor (GSIF). In this case, λ only depends on the corner angle Ψ, and *K* depends on the boundary conditions of the finite problem [29,30]. Asymptotic analyses are commonly employed to assess crack initiation when using square-ended flat punches [30,31]. The contact pressure along the contact area can be obtained by different ways although the simplest solution may be the one given by Hills et al. [32] for squared edge frictionless problems:

$$\frac{bp(x)}{P} = \frac{1}{\pi\sqrt{1-\left(\frac{x}{b}\right)^2}} \tag{5}$$

2.3 Flat punch with rounded edges to flat surface contact configuration (FTFR)

The flat indenter with rounded edges to plane contact configuration is a formally a complete contact configuration, although in some cases the contact behaviour resembles an incomplete contact. This type of contact can be understood as a transition between both contact configurations reviewed above. Fig. 1 shows a sketch of this contact configuration where *b* and *a* represent the flat and total half-widths of contact, respectively. The transition is defined by the ratio of *b/a*, as it will be analytically shown below.

The analytical solution of the contact pressure was firstly obtained by Ciavarella et al. [33]. The normalized contact pressure is given in Eq. 6, being $\sin(\phi_0) = b/a$ and using $x = b\frac{\sin(\phi)}{\sin(\phi_0)}$. Fig. 2 shows the normalized contact pressure distribution for the three contact configurations reviewed in this section. Note that three contact pressure distributions with different ratios *b/a* have been plotted for the case of rounded punch. When *R* is minimal and the ratio of *b/a* is close to 1, the contact status is similar to the square-ended punch and as shown in Fig. 2, and the contact pressure distribution tends to a complete contact configuration. On the other side, when *R* is large enough, and the flat length contact is relatively small, the contact status is more similar to the contact status produced by a cylindrical pad.

$$\frac{ap(\phi)}{P} = \frac{2/\pi}{\pi - 2\phi_0 - \sin(2\phi_0)} \times \left\{(\pi - 2\phi_0)\cos(\phi) + \log\left[\left|\frac{\sin(\phi+\phi_0)}{\sin(\phi-\phi_0)}\right|^{\sin(\phi)} \times \left|\tan\frac{\phi+\phi_0}{2}\tan\frac{\phi-\phi_0}{2}\right|^{\sin(\phi_0)}\right.\right. \quad (6)$$

3. Methodology

3.1. Mesh Control Analysis Scheme

In this section, a summary of the analysis scheme of the TCD with mesh control approach and TCD with point method used in this work is presented. Fig. 3 sketches both fatigue life assessment methodologies. A very refined mesh is required for an accurate prediction of the stress field when using finite element models in fretting fatigue problems. In the TCD with point method, the fluctuating stresses at a distance of *L*/2 from the surface need to be recorded, where *L* is the critical distance. A mesh sensitivity analysis was carried out on the SWT parameter calculated through the critical plane analysis at a depth of *L*/2 from the hot spot. Successive analyses were performed reducing the element size in such a way that in all cases the centroid depth matched *L*/2. Convergence was assumed to be achieved when the relative difference between two consecutive analyses was below 5%. After conducting the sensitivity study for all cases under study, an element size was defined for the TCD, being the optimum elements: *L*/5 for incomplete contact case and *L*/11 (stresses are recorded at the sixth element layer) for the complete contact. In this work, the element size for CTF, FTFR and FTFS was 0.0086 mm, 0.0051 mm and 0.0016 mm. In the TCD with mesh control approach, the element size was changed between 1- and 6-times *L*, and the SWT parameter (the fatigue indicator parameter, FIP, as explained in section 3.3) was contrasted to the value obtained

through TCD with PM approach by means of relative error. Therefore, it is possible to seek the optimum element size for each case. Note that in the TCD with mesh control input stresses for the critical plane analysis are recorded from nodes and in the TCD with point method the stresses are recorded from centroids. As depicted in Fig. 3, the main objective of TCD-MC is to estimate a similar FIP to TCD-PM by means of controlling the element size. In this way, the FIP value obtained at the hot spot (TCD-MC) is the same as the one calculated at L/2 from the hot spot with a more refined mesh (TCD-PM). The reader is referred to [8] for further details where a full description of the methodology was presented.

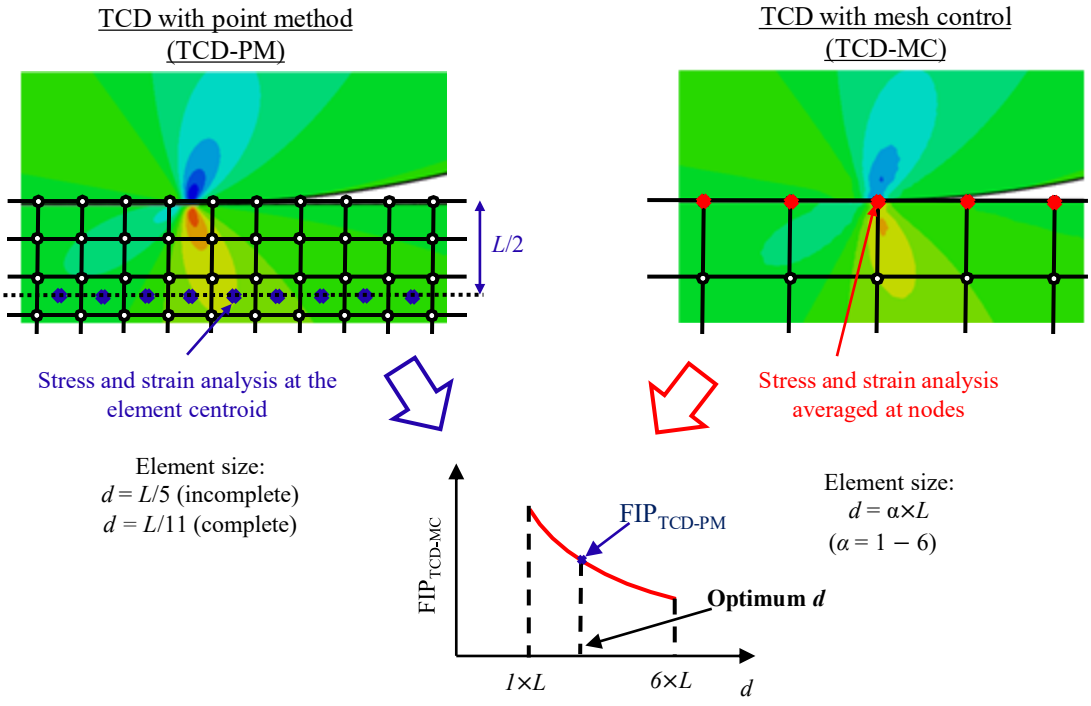

Fig. 3. Adopted analysis scheme to define the optimum element size *d* for the TCD with the mesh control method. FIP_{TCD}= fatigue indicator parameter, calculated using the TCD with point method (TCD-PM) or TCD with mesh control (TCD-MC) [8]. Note that the sketched mesh sizes do not correspond with the represented numerical in-plane shear stress field solution.

3.2. Experimental campaign

To analyse the viability of using the TCD mesh control approach for fretting fatigue life prediction the numerical results must be compared with actual experimental data for each of the contact configurations covered.

3.2.1. Cylinder-on-Flat 2024-T3

This section refers to the incomplete contact case used as reference in the present study, the most frequently described and well-established cylindrical contact. This contact has been widely studied for a wide range of high strength aluminium and titanium alloys usual in the aerospace industry under varied test conditions.

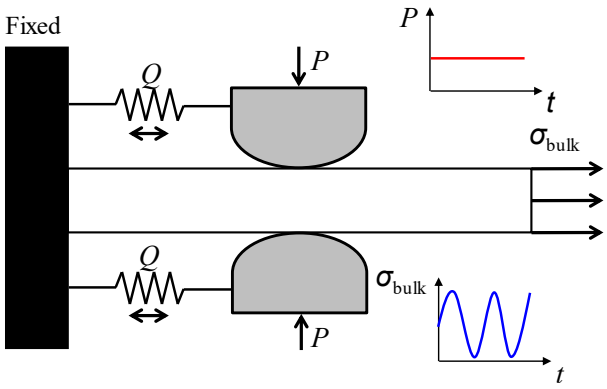

Fig. 4: Fretting fatigue test configuration used by Talemi et al. [34].

Usually, the cylindrical pads are pressed against a rectangular dog-bone specimen and a constant amplitude bulk stress is applied to the specimen, as shown in Fig. 4. Hence, a tangential force Q is generated between the cylindrical pad and the specimen. With this configuration, the experimental data used in the present work was generated by Talemi et al. [34]. A 100 kN EHS servo-hydraulic machine was employed. A test campaign in a 2024-T3 aluminium with variable bulk stress amplitude was carried out with a positive stress ratio (R_σ = 0.1). For each test, the tangential force Q was proportional to the cyclic remote stress and fully reversed (R_Q = -1) because the normal load was applied after loading the mean bulk axial load. The following table summarises the test conditions of the reported data. All tests were performed under a constant normal load per unit of thickness of 135.75 N/mm.

Test condition	σ_{bulk} [MPa]	Q_{max} [N/mm]	N_f [cycles]
CTF1	100	38.79	1407257
CTF2	115	46.56	1105245
CTF3	135	55.93	358082
CTF4	135	48.89	419919
CTF5	160	48.43	245690
CTF6	190	82.54	141890
CTF7	205	80.53	114645
CTF8	220	66.79	99607
CTF9	220	79.46	86647

Table 1: Load conditions for tests (maximum value of the cyclic axial load is reported) carried out by Talemi et al. [34].

3.2.2. Flat-on-Flat with Sharp Edges 7075-T6

The second configuration that has been taken into account is a flat-to-flat contact with sharp edges. Such a configuration has been experimentally characterized and numerically predicted by Sabsabi et al. [35], who used a uniaxial servo-hydraulic fatigue test machine with a load capacity of ±100 kN on dog-bone-shaped test specimens made of 7075-T6 aluminum alloy and rectangular section (T-S orientation). On these specimens, Sabsabi et al. [35] performed fretting fatigue tests with floating square-ended indenters in a partial slip regime (see Fig. 5).

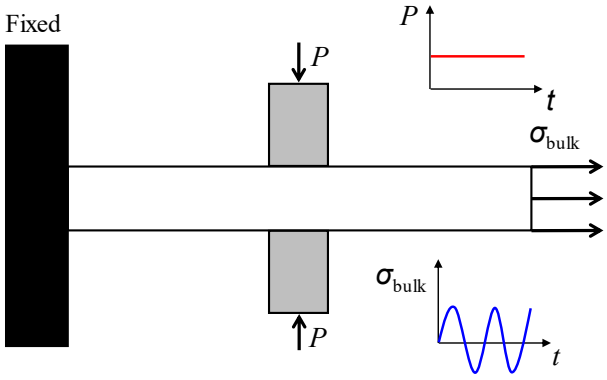

Fig. 5: Fretting fatigue test configuration used by Sabsabi et al. [35].

Indenters were manufactured by milling but not ground and the same indenter surface condition was essentially achieved in all the tests. Avoiding any other manufacturing process guaranteed an optimal even surface and sharp edges that were measured to be of the order of 10 µm, presenting local imperfections due to the microstructure of the material and the grain size. With this configuration the cyclic bulk loading was performed at constant amplitude, stress ratio R = -1 at a frequency of 15 Hz. Fifteen loading combinations were performed and reported, varying the normal and bulk loads as summarized in Table 2. The nominal contact pressure is defined as $\sigma_P = P/2at$ where $2a$ is the contact width and t the specimen and indenter thickness. Lastly, the load ratio is defined as the fraction between the normal load and the maximum bulk load applied in each test condition.

Test code	σ_P [MPa]	σ_{Bulk} [MPa]	Load ratio [-]	N_f [cycles]
FTFS1	40	110	0.36	105,958
FTFS2	40	130	0.31	64,764
FTFS3	40	150	0.27	35,181
FTFS4	40	170	0.24	24,306
FTFS5	40	190	0.21	12,509
FTFS6	80	110	0.73	92,259
FTFS7	80	130	0.62	47,714
FTFS8	80	150	0.53	32,905
FTFS9	80	170	0.47	27,391

FTFS10	80	190	0.42	9,590
FTFS11	160	110	1.45	82,549
FTFS12	160	130	1.23	43,567
FTFS13	160	150	1.07	25,872
FTFS14	160	170	0.94	23,046
FTFS15	160	190	0.84	8,760

Table. 2: Loading conditions of fretting fatigue tests performed by Sabsabi et al. [35].

3.2.3. Flat-on-flat with rounded edges Ti-6Al-4V

Finally, the tests carried out by Jin and Mall using a dog bone specimen made by Ti-6Al-4V clamped to a flat punch with rounded edges of the same material were analysed [36]. The fretting fatigue apparatus consisted of two independent servo-hydraulic actuators (13kN and 100kN). An actuator is attached to the dog-bone specimen producing the cyclic bulk load and the other actuator is attached to the fretting fixture in order to control the cyclic tangential load and displacement. Moreover, an extensometer was placed in the fretting fixture to record the pad tangential displacement. Further details of the test configuration can be found in the original publication [36]. Due to the fretting configuration, Jin and Mall produced fretting fatigue tests with large cyclic pad tangential displacement (see Fig. 6). Under these conditions, wear is usually significantly large and may affect the fatigue crack initiation and propagation, delaying the crack initiation stage due to the removal of incipient damage. Thus, numerical models based on non-local stress, such as TCD, which do not incorporate wear of the surfaces usually predict too conservative results [9]. However, TCD can be satisfactory applied in combination with wear models [9,14]. For this reason, we have only considered test conditions under reported stick-slip regime (see Table 3). All tests were performed using a sinusoidal bulk load with maximum 550 MPa and stress ratio 0.03. Normal load was prescribed before cyclic bulk load. Tests were performed under constant load P at two values: 1334 N and 400 N.

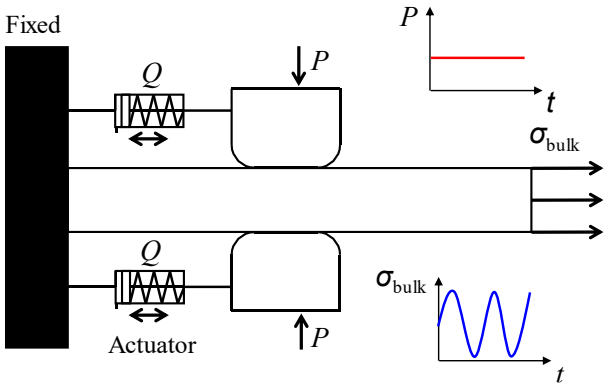

Fig. 6: Fretting fatigue test configuration used by Jin and Mall [36].

Test code	P [N]	Δd_{aap} [μm]	Q_{max} [N]	Q_{min} [N]	Q_{max}/P	$\Delta\delta$ [μm]	N_f
FTFR1	1334	0	943	-778	0.71	36	55206
FTFR2	1334	73	1108	-1001	0.83	40	192283
FTFR3	4000	0	1352	-445	0.34	30	33547
FTFR4	4000	294	1957	-1868	0.49	40	26684
FTFR5	4000	441	2331	-2406	0.58	46	75189
FTFR6	4000	147	1450	-1397	0.36	33	36790

Table. 3: Loading conditions and fretting fatigue life until failure of tests performed by Jin and Mall [36].

3.2.4. Material data

Table 5 shows the material properties of the reported data whereas Table 4 presents the material fatigue constants of the materials obtained from the published literature. The corresponding *L* critical distance values were computed using the previously shown Eq. 1. Note that *L* was calculated using constants at different load ratios because of the lack of material data. As shown in Table 5, a constant coefficient of friction was assumed for AL2024-T3 and 7075-T6 aluminium alloys. However, based on the results obtained in [36] two coefficients were assumed for Ti-6Al-4V: 0.8 for a normal load of 4000 N and 1 for a normal load of 1334 N.

Material	σ_f' [MPa]	b [-]	ε_f' [-]	c [-]	ΔK_{th} (R=0) [MPa·m$^{1/2}$]	$\Delta\sigma_0$ (R=-1) [MPa]	N_A [Cycles]	L [μm]
Al 2024-T3 [37] [34]	1194	-0.133	-	-	3.2	276	$5\cdot10^8$	42.79
7075-T6 [38][39]	1917	-0.176	0.156	-0.526	2.2	166	NA	56
Ti-6Al-4V [36] [9]	2030	-0.104	0.841	-0.688	4.2	569	NA	17.34

Table. 4: Plain fatigue material data.

Material	**Elastic modulus *E* [GPa]**	**Poisson's ratio *ν* [-]**	**Coefficient of friction *μ* [-]**
Al 2024-T3 [34]	72.1	0.33	0.65

7075-T6 [35]	72	0.3	0.8
Ti-6Al-4V [36]	126	0.32	0.8 - 1

Table. 5: Material mechanical properties.

3.3. Fatigue Indicator Parameter

In this work, the critical plane approach was evaluated using the Smith-Watson-Topper (SWT) parameter as the fatigue indicator parameter [37]. The SWT is a mode I type failure criterion. The SWT parameter is defined as the maximum, over all possible directions, of the product of maximum normal stress ($\sigma_{n,max}$) and normal strain amplitude ($\varepsilon_{n,a}$):

$$\mathrm{SWT} = (\sigma_{n,max}\epsilon_{n,a})_{max} = \frac{\sigma_f^{'2}}{E}\left(2N_f\right)^{2b} + \sigma_f^{'}\epsilon_f^{'}\left(2N_f\right)^{b+c} \tag{7}$$

where $\sigma_f^{'}$ is the fatigue strength coefficient, b is the fatigue exponent, E is the elastic modulus, N_f is the number of cycles to failure, $\epsilon_f^{'}$ is the fatigue ductility coefficient and c is the fatigue ductility exponent. As previously said, FIP parameters are usually evaluated within the critical plane approach. This approach identifies the plane with the maximum fatigue damage at any material point. In the case of SWT parameter, the maximum value of the FIP must be identified, i.e. $\left(\sigma_{n,max}\varepsilon_{n,a}\right)_{max}$. The fluctuating deformations of the solid can be considered as purely elastic in problems whose applied loads are not large enough to exceed the material yield stress. In this case, the previous equation is simplified to:

$$\mathrm{SWT} = (\sigma_{n,max}\epsilon_{n,a})_{max} = \frac{\sigma_f^{'2}}{E}\left(2N_f\right)^{2b} \tag{8}$$

3.4. FE modelling

The finite element models were developed in Abaqus© Standard as 2D plane strain models using 4-node quadrilateral elements with full integration (CPE4). In all models, a multi-point constraint (MPC) was applied on nodes located at top edge of the indenter in order to distribute the normal load P and to avoid the indenter rotation. In addition, the Lagrange multipliers algorithm was used to model friction between indenter and specimen. A sketch of the three models is presented in Fig. 7. Only half domain was modelled due to symmetry conditions for the configurations flat-to-cylinder (CTF) and flat-to-flat with rounded edges (FTFR). On the other hand, a quarter of the test was modelled in the flat-to-flat with square edges contact configuration (FTFS). In this case, there is no developed tangential load because the fretting rig is floating. However, the tangential load Q is

introduced in the models with the configurations flat-to-cylinder contact and flat-to-flat with rounded edges through the application of a cyclic reaction load σ_R on the other edge of the specimen as sketched in Fig. 7. In the CTF configuration, the stress ratio of the tangential load is -1, but in the FTFR the tangential load is not constant as seen in Table 3. However, it is possible to introduce the exact maximum and minimum values in the numerical model through the reaction axial load.

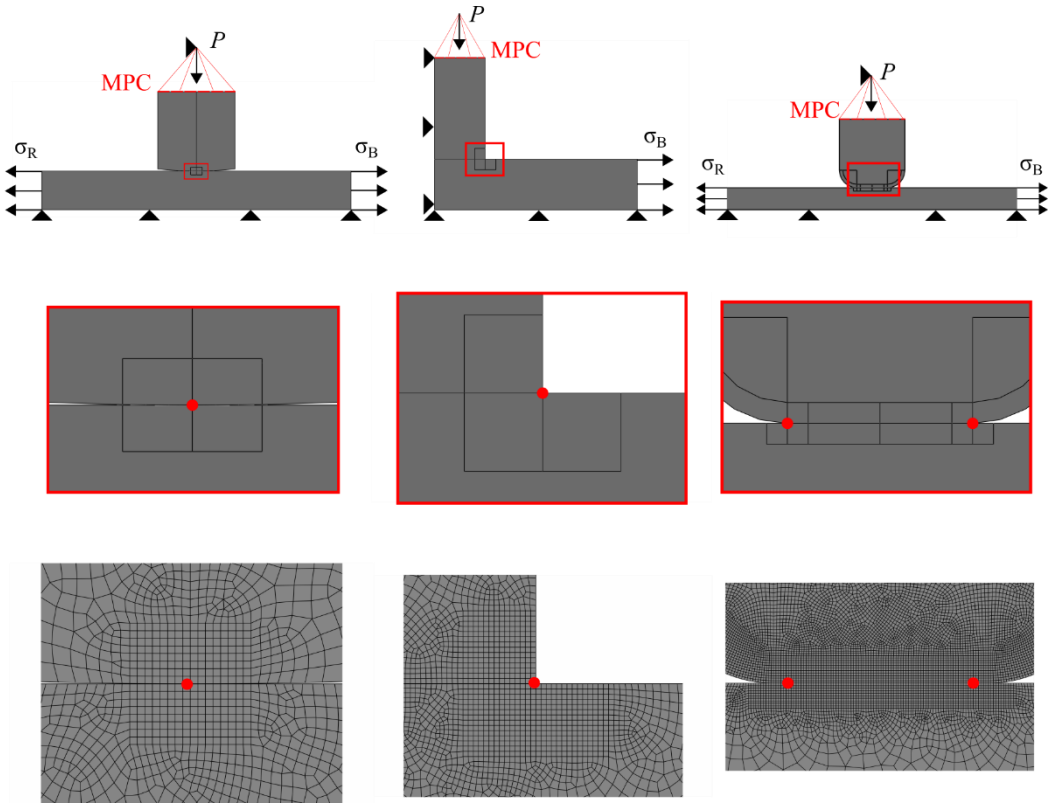

Fig. 7: From left to right: sketch of the numerical model boundary conditions and mesh partition strategies for the three fretting fatigue tests studied in this work: cylinder-to-flat contact (CTF), flat-to-flat with square edges contact (FTFS) and flat-to-flat with rounded edges contact (FTFR).

Regarding the mesh topology, some considerations need to be addressed in order to correctly apply the mesh control approach in fretting fatigue problems. We recommend creating partitions in such a way that the mesh is symmetric with respect to the contact region. Furthermore, in flat-to-flat contact is recommended to locate a node at the transition point as sketched in Fig. 7 (strategic node positions in each model are indicated with a red point). Lastly, regular meshes must be used surrounding the contact area of at least 0.5 mm depth or ten times the mesh control element size.

4. Results and discussion

Results are presented in 3 different subsections. First of all, the results of a parametric analysis of different synthetic critical distance sizes on the optimum mesh size using TCD with MC are presented for the three test configurations. The synthetic critical distance range covers the critical distance values of common materials used in applications where fretting fatigue occurs. Next, the results of the relative error obtained using the mesh control with TCD approach in comparison with the TCD with point method approach are presented for all test configurations and loading conditions reported in section 3 in order to seek the optimum mesh size. Finally, lifetime predictions using TCD with PM and TCD with MC (note that in this case only one optimum mesh size is applied for the life assessment) are compared with experimental evidence.

4.1. Synthetic *L* data analysis

The length of the critical distance may be the most significant parameter affecting the lifetime assessment when using the TCD approach, especially in the presence of severe stress gradient as in fretting fatigue problems. Thus, we have performed a parametric analysis of different critical distance values for the three contact configurations which cover the typical values found in materials utilised in fretting fatigue applications. The studied loading conditions are: CTF5 loading condition for the CTF contact configuration, FTFS1 loading condition for FTFS contact and FTFR1 loading condition for FTFR contact. Critical distance length values were selected to cover typical ranges corresponding to high-strength materials used in fretting fatigue: 10, 30, 50 and 70 μm. In total, two hundred and forty simulations were carried out: 20 mesh sizes with 4 synthetic critical lengths in 3 different problems. The aim of this study was to assess the effect of the critical distance value in the optimum size used for the TCD with MC approach. Therefore, the SWT parameter was estimated using the TCD with PM at a distance of $L/2$ from the hot spot using a refined mesh. Next, the SWT parameter is calculated directly at the hot spot using different meshes with an element size equal to α times L for each synthetic L length. Finally, the relative error between the estimated SWT by the TCD with PM and the TCD with MC approach using different mesh sizes is carried out. Fig. 8 shows the relative error for the three contact configurations. The relative error is calculated as follows:

$$Relative\ error\ SWT\ [\%] = \frac{SWT_{TCD-MC} - SWT_{TCD-PM}}{SWT_{TCD-PM}} 100 \tag{9}$$

As can be seen, a similar trend was observed for the three contact configurations. A small α (i.e., small element size) produces an overestimation of the SWT parameter: the average of the stress gradient within an element next to the hot-spot is larger because the mesh is more refined with small

elements. It can be observed that an erratic behaviour can be found in the flat-to-cylinder contact configuration (Fig. 8. a) because of the influence of the relative distance of nodes to the contact edge when changing the mesh size (more details can be found in [8]). However, this erratic behaviour disappears in the flat-to-flat with square edges (Fig. 8. b) because there is always a node located at the hot-spot due to the contact geometry and mesh partitions. Furthermore, this erratic behaviour appears again in the flat-to-flat with rounded edges, but with less severity. This was expected as this contact type is a hybrid between the cylindrical contact and flat to flat with sharp edges, so-called as nearly complete contact, as mentioned above.

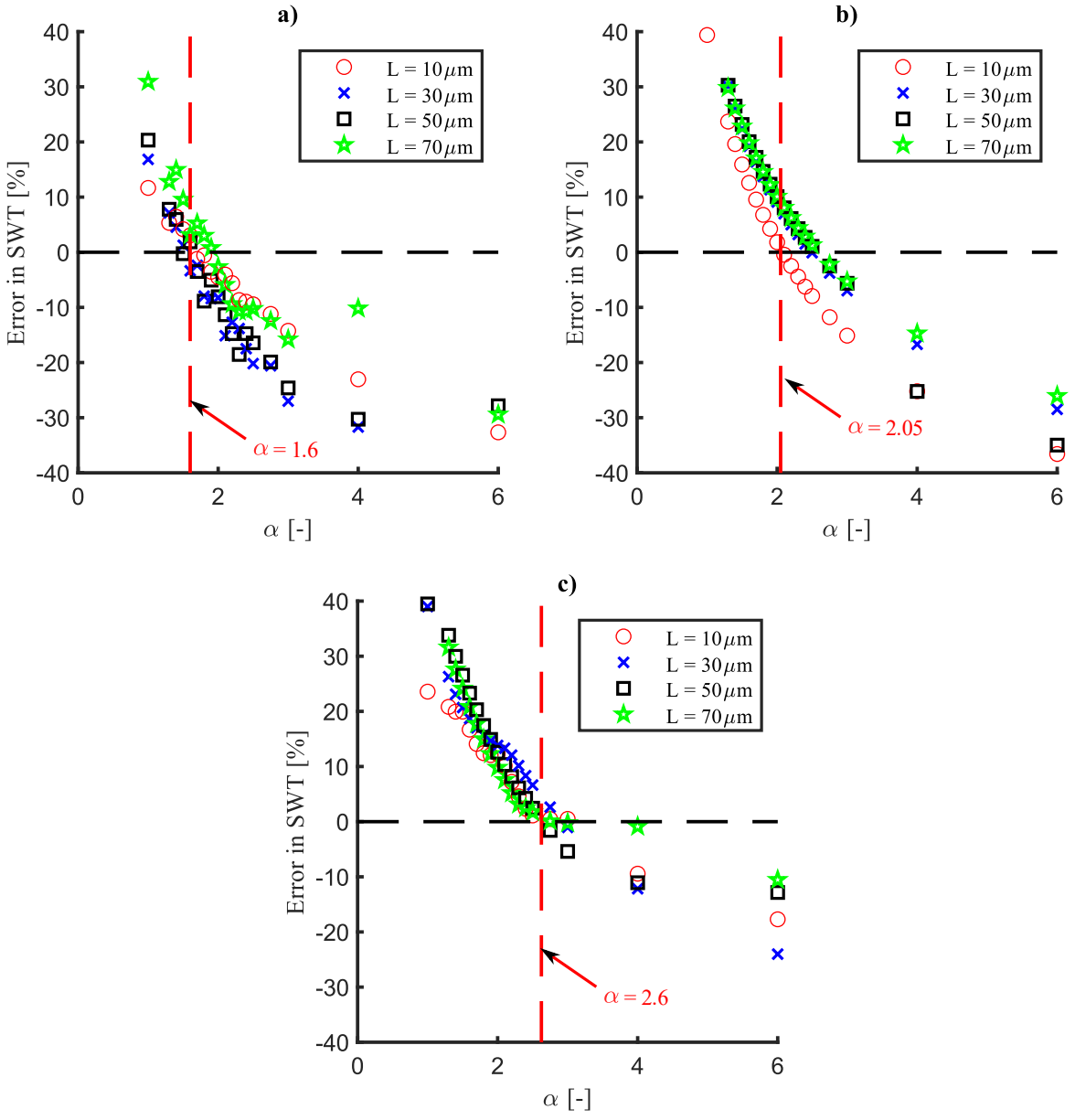

Fig. 8: Synthetic L analysis for the three contact configurations under study: (a) CTF (b) FTFS (c) FTFR.

Although the optimum size is below 2 for the CTF contact, the optimum size appears to be between 2 and 3 for the flat-to-flat contacts (a vertical red dashed line marks the transition between positive to negative relative errors). The variability of the optimum size for each contact configuration is not significantly large, but it is important to take it into account when analysing flat-to-flat contacts for accurate lifetime predictions.

4.2. TCD with point method vs. TCD with mesh control

In this subsection, the mesh control approach is applied to the experimental tests described in section 3. In total, six hundred simulations were run, corresponding to thirty tests with twenty different mesh sizes each. Fig. 9 shows the relative error in SWT obtained with the MC approach for different element sizes. The optimum size for tests with FTFS and FTFR significantly changes for different loading cases in comparison with the CTF contact. This effect is more pronounced in tests using FTFS contact configuration where the optimum element size moves from 2 to a value greater than 6, although in FTFR the optimum size value seems more limited in a range from 2 to 4. The main explanation for this outcome is because of the high sensitivity to load conditions of the contact status along the contact interface, especially close to the edges of complete contacts. It has been observed in the FE models that for small ratios of the normal load and bulk load the contact edges lift (see Fig. 10). Therefore, the stress singularity vanishes, and the contact behaves similar to an incomplete contact. In these cases, the optimum size moves to a value around 2. On the other hand, when the ratio between the normal load and bulk load is large enough to avoid edge lifting, the optimum size value increases.

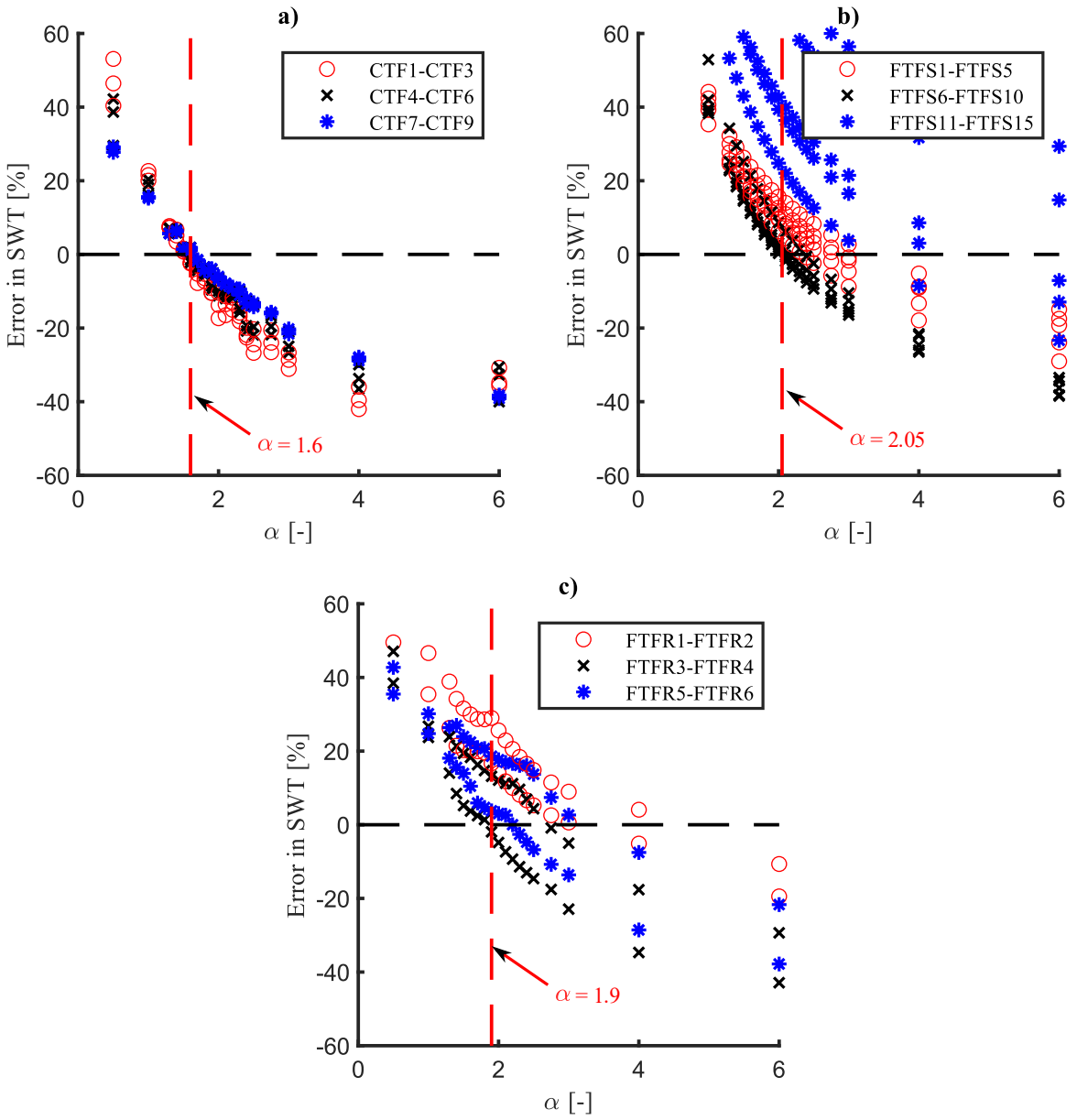

Fig. 9: Relative error between SWT parameter calculated by TCD with PM and TCD with MC at different mesh sizes (a) CTF contact L = 42.79 µm (b) FTFS L = 56 µm (c) FTFR L = 17.34 µm.

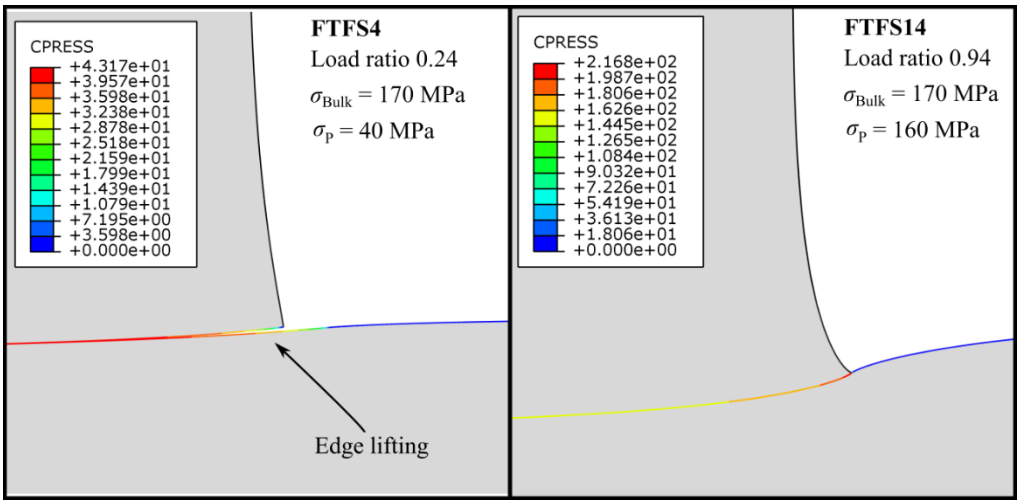

Fig. 10: Contact pressure distribution in MPa around the contact edge at maximum bulk load in FTFS contact for two loading conditions: FTFS4 and FTFS14. Note that deformed shapes have been scaled (x100) to enable the visualization.

In order to obtain conservative predictions with the TCD with MC approach in comparison to TCD with PM and as a rule of thumb, an optimum size of 1.6 would be enough to overestimate the SWT parameter predicted using TCD with MC. Using an optimum size of 1.6, the relative error in SWT is always positive. Note that although the results pointed out that a variable optimum size higher than 1.6 should be used for complete contacts, using a unique value for all cases, always from the safest position, is just a simplification of the problem to make the mesh control approach a more general and straightforward method.

A summary of the relative errors is presented in Fig. 11 for the three contact configurations with a fixed element size of 1.6 times L. As it can be seen, the relative errors are below 30% for CTF and FTFR, but significantly large for FTFS up to 80%. However, we can see that errors are mainly positive which directly implies that predicted results by TCD-MC must be more conservative than TCD-PM. In addition, the relative error median is close to 20%.

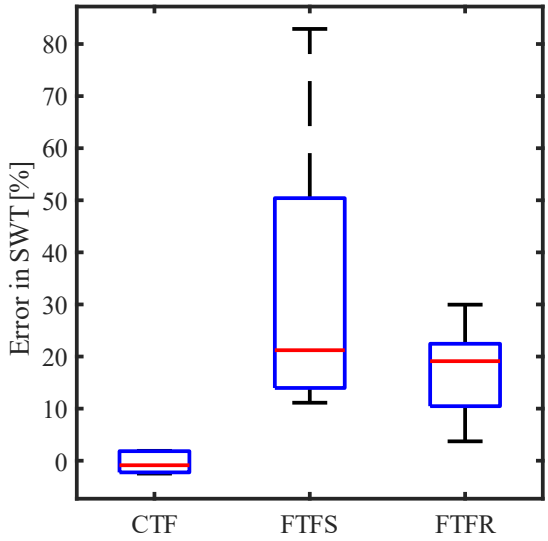

Fig. 11: Predicted relative errors obtained for the three contacts for an element size d = 1.6 x L (median, minimum and maximum values are illustrated to show the whole range of error considering all loading cases).

4.3. Life assessment using TCD with point method and TCD with mesh control

In this subsection, the lifetime correlation results of the three experimental campaigns along with the life predictions using TCD with PM and TCD with MC are presented. Fig. 12 shows the experimental results against predictions corresponding to the three contact configurations using TCD with PM and TCD with MC. Note that lifetime predictions with TCD-MC are calculated using an element size d = 1.6 x L. Additionally, a purely elastic prediction is performed for all contact configurations using Eq. 7. Note that yield stress is theoretically reached for any case in FTFS contact configuration such as in blunt notches due to the elastic stress singularity caused by the sharp geometric change, either in the contact corner or in the blunt notch. However, the plasticity is negligible in some cases because the plastic area is usually highly localized due to the severe stress gradients, and the small-scale yielding assumption can be considered [35,40]. The results show the ability of the TCD method for fretting fatigue lifetime prediction. As expected, the results predicted by TCD with MC are more conservative than lifetime predictions performed by TCD with PM. Note that some results in the FTFR are very conservative for both TCD approaches: TCD-MC and TCD-PM. This is probably due to the experimental tests used in this study (see Section 3.2.3). The tests in FTFR [35] produced large cyclic pad tangential displacement, with significant wear that delays the crack initiation stage due to

the removal of incipient damage. This phenomenon has not been taken into account in the corresponding numerical model, leading to too conservative results. Note that this is a significant limitation for accurate predictions when using the TCD with PM and MC. On the contrary, results for FTFS are based on tests with only partial slip, with much less wear and therefore the numerical model is closer to the actual behaviour, leading to more accurate results.

As seen in previous section, the TCD with MC has some limitations in flat-to-flat contacts due to the scatter of the optimum size values, particularly for FTFS contacts. However, the approach is still promising to fatigue strength assessment, as a value of d = 1.6 x L will lead to conservative results with negligible computation time. As mentioned earlier, this is important for industry applications as usually a fast and simple method is desired. The TCD with PM application to FTFR took approximately 7 hours to solve one case (finite element analysis and post-processing critical plane approach) using 12 CPUs at 3.5 GHz. However, the same case in the TCD with MC took around 8 minutes, which means a reduction of approximately 98%. In the previous study with CTF contact [8], a computational time reduction of 97% was obtained which is similar to the value obtained with FTFR and FTFS contacts in this work.

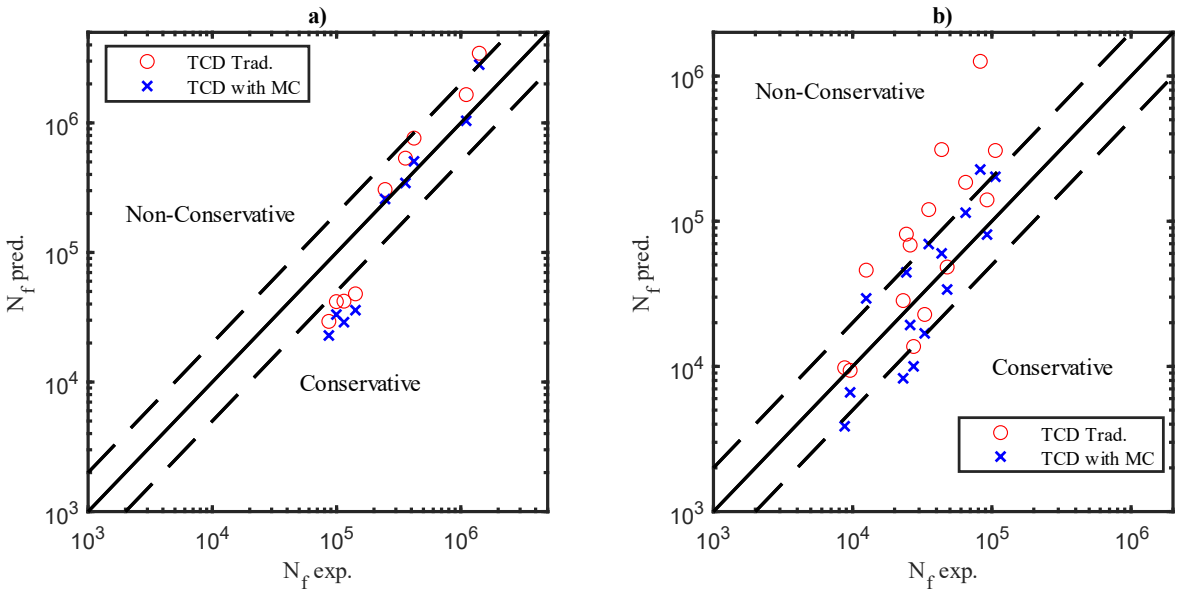

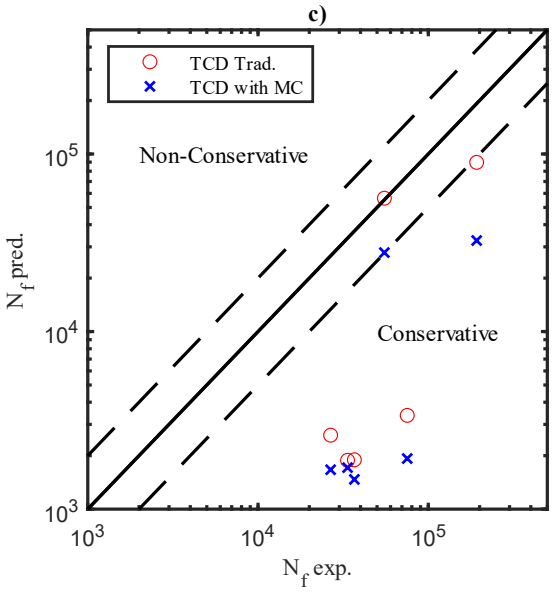

Fig. 12: Life assessment obtained by TCD with PM and TCD with MC using a mesh size of 1.6 times *L*: (a) CTF (b) FTFS (c) FTFR

5. Conclusions

In this work, the viability of the TCD with mesh control approach for fretting fatigue application for two different contact types was analysed: FTFS and FTFR. In addition, the results are compared with a CTF contact configuration previously analysed. The following conclusions can be drawn from this study

- The TCD with MC can be successfully applied to fretting fatigue life assessment in complete and nearly complete contacts using a mesh size of 1.6 times the critical distance length. However, it is expected that more conservative results would be predicted with the TCD with MC than with the TCD with PM.
- Optimum mesh size in TCD with MC showed variability in complete and nearly complete contacts when compared to incomplete contacts. For this reason, accurate predictions with TCD with MC in complete contacts may be possible but using different optimum mesh sizes for different loading ratios. However, and from the point of view of the authors, finding the optimum mesh sizes may be a cumbersome process. Instead, it is recommended to get a conservative prediction for complete contacts using the mesh size obtained for incomplete contacts (1.6 times the critical distance length).

- The computational time using the TCD with MC showed again a significant decrease in comparison with the TCD with PM up to 98%. In this way, the approach is still promising for fatigue strength assessment and near future work will include 3D fretting fatigue problems where computational time is critical.

Further comparisons with other experimental tests are recommended in order to confirm the trends and values found in this work.

Acknowledgments

This research was funded by the FEDER programme and the Spanish Ministry of Science and Innovation, under project PID2020-118480RB-C21 / AEI / 10.13039/501100011033. The funding of the Generalitat Valenciana, Programme PROMETEO 2021/046 and Universitat Politècnica de València, Programme PAID-10-21 is also acknowledged.

References

[1] D.A. Hills, D. Nowell, Mechanics of Fretting Fatigue, Kluwer Academic Publishers, 1994.

[2] H. Tang, D. Cao, H. Yao, M. Xie, R. Duan, Fretting fatigue failure of an aero engine turbine blade, Eng. Fail. Anal. 16 (2009) 2004–2008. https://doi.org/10.1016/J.ENGFAILANAL.2008.07.010.

[3] D.A. Hills, H.N. Andresen, Mechanics of Fretting and Fretting Fatigue, Springer International Publishing, Cham, 2021. https://doi.org/10.1007/978-3-030-70746-0.

[4] D. Dini, D. Nowell, I.N. Dyson, The use of notch and short crack approaches to fretting fatigue threshold prediction: Theory and experimental validation, Tribol. Int. 39 (2006) 1158–1165. https://doi.org/10.1016/J.TRIBOINT.2006.02.033.

[5] M. Ciavarella, A 'crack-like' notch analogue for a safe-life fretting fatigue design methodology, Fatigue Fract. Eng. Mater. Struct. 26 (2003) 1159–1170. https://doi.org/10.1046/J.1460-2695.2003.00721.X.

[6] M. Ciavarella, F. Berto, A simplified extension of the Crack Analogue model for fretting fatigue with varying normal load, Theor. Appl. Fract. Mech. 91 (2017) 37–43. https://doi.org/10.1016/J.TAFMEC.2017.03.011.

[7] S. Fouvry, P. Kapsa, L. Vincent, A Multiaxial Fatigue Analysis of Fretting Contact Taking Into Account the Size Effect, in: Frett. Fatigue Curr. Technol. Pract., ASTM International, 100 Barr Harbor Drive, PO Box C700, West Conshohocken, PA 19428-2959, 2000: pp. 167-167–16. https://doi.org/10.1520/STP14728S.

[8] A. Zabala, D. Infante-García, E. Giner, S. Goel, J.L. Endrino, I. Llavori, On the use of the theory of critical distances with mesh control for fretting fatigue lifetime assessment, Tribol. Int. 142 (2020) 105985.

https://doi.org/10.1016/j.triboint.2019.105985.

[9] I. Llavori, A. Zabala, M.A. Urchegui, W. Tato, X. Gómez, A coupled crack initiation and propagation numerical procedure for combined fretting wear and fretting fatigue lifetime assessment, Theor. Appl. Fract. Mech. 101 (2019) 294–305. https://doi.org/10.1016/J.TAFMEC.2019.03.005.

[10] D. Taylor, Geometrical effects in fatigue: a unifying theoretical model, Int. J. Fatigue. 21 (1999) 413–420. https://doi.org/10.1016/S0142-1123(99)00007-9.

[11] D. Taylor, The theory of critical distances, Eng. Fract. Mech. 75 (2008) 1696–1705. https://doi.org/10.1016/J.ENGFRACMECH.2007.04.007.

[12] V.S.R. Adriano, J.M.G. Martínez, J.L.A. Ferreira, J.A. Araújo, C.R.M. da Silva, The influence of the fatigue process zone size on fatigue life estimations performed on aluminum wires containing geometric discontinuities using the Theory of Critical Distances, Theor. Appl. Fract. Mech. 97 (2018) 265–278. https://doi.org/10.1016/J.TAFMEC.2018.09.002.

[13] A.L. Pinto, J.A. Araújo, R. Talemi, Effects of fretting wear process on fatigue crack propagation and life assessment, Tribol. Int. 156 (2021). https://doi.org/10.1016/J.TRIBOINT.2020.106787.

[14] R.A. Cardoso, T. Doca, D. Néron, S. Pommier, J.A. Araújo, Wear numerical assessment for partial slip fretting fatigue conditions, Tribol. Int. 136 (2019) 508–523. https://doi.org/10.1016/J.TRIBOINT.2019.03.074.

[15] J.J. Chen, L. Liu, S.X. Li, S.R. Yu, Y.N. He, Experimental and numerical investigation on crack initiation of fretting fatigue of dovetail, Fatigue Fract. Eng. Mater. Struct. 41 (2018) 1426–1436. https://doi.org/10.1111/FFE.12787.

[16] T. Hattori, V.T. Kien, M. Yamashita, Fretting fatigue life estimations based on fretting mechanisms, Tribol. Int. 44 (2011) 1389–1393. https://doi.org/10.1016/J.TRIBOINT.2010.10.020.

[17] S.L. Sunde, B. Haugen, F. Berto, Experimental and numerical fretting fatigue using a new test fixture, Int. J. Fatigue. 143 (2021) 106011. https://doi.org/10.1016/J.IJFATIGUE.2020.106011.

[18] V.S.R. Adriano, J.M.G. Martínez, J.L.A. Ferreira, J.A. Araújo, C.R.M. da Silva, The influence of the fatigue process zone size on fatigue life estimations performed on aluminum wires containing geometric discontinuities using the Theory of Critical Distances, Theor. Appl. Fract. Mech. 97 (2018) 265–278. https://doi.org/10.1016/J.TAFMEC.2018.09.002.

[19] T. Gailliegue, T. Doca, J.A. Araújo, J.L.A. Ferreira, Fretting life of the Al7050-T7451 under out-of-phase loads: Numerical and experimental analysis, Theor. Appl. Fract. Mech. 106 (2020) 102492. https://doi.org/10.1016/J.TAFMEC.2020.102492.

[20] D. Infante-García, E. Giner, H. Miguélez, M. Abdel Wahab, Numerical analysis of the influence of micro-voids on fretting fatigue crack initiation lifetime, Tribol. Int. 135 (2019) 121–129. https://doi.org/10.1016/j.triboint.2019.02.032.

[21] F. Vargiu, D. Sweeney, D. Firrao, P. Matteis, D. Taylor, Implementation of the Theory of Critical Distances using mesh control, Theor. Appl. Fract. Mech. 92

(2017) 113–121. https://doi.org/10.1016/J.TAFMEC.2017.05.019.

[22] H. Hertz, Ueber die Berührung fester elastischer Körper, J. Fur Die Reine Und Angew. Math. 1882 (1882) 156–171. https://doi.org/10.1515/crll.1882.92.156.

[23] K.L. Johnson, One Hundred Years of Hertz Contact, Proc. Inst. Mech. Eng. 196 (1982) 363–378. https://doi.org/10.1243/pime_proc_1982_196_039_02.

[24] C. Cattaneo, Sul contatto di due corpi elastici: distribuzione locale degli sforzi, Rend. Dell'Aecademia Naz. Dei Lincei. 27 (1938) 342–348. http://dx.doi.org/10.1016/0043-1648(92)90266-B (accessed February 18, 2020).

[25] R.D. Mindlin, Compliance of Elastic Bodies in Contact, in: Collect. Pap. Raymond D. Mindlin Vol. I, 1989: pp. 197–206. https://doi.org/10.1007/978-1-4613-8865-4_24.

[26] D. Nowell, D.A. Hills, Mechanics of fretting fatigue tests, Int. J. Mech. Sci. 29 (1987) 355–365. https://doi.org/10.1016/0020-7403(87)90117-2.

[27] T.R. Newton, S.N. Melkote, T.R. Watkins, R.M. Trejo, L. Reister, Investigation of the effect of process parameters on the formation and characteristics of recast layer in wire-EDM of Inconel 718, Mater. Sci. Eng. A. 513–514 (2009) 208–215. https://doi.org/10.1016/j.msea.2009.01.061.

[28] M.L. Williams, Stress Singularities Resulting From Various Boundary Conditions in Angular Corners of Plates in Extension, J. Appl. Mech. ASME. 19 (1952) 526–528.

[29] E. Giner, D.A. Hills, F.J. Fuenmayor, Complete Elastic Contact Subject to Cyclic Shear in Partial Slip, J. Eng. Mech. 131 (2005) 1146–1156. https://doi.org/10.1061/(asce)0733-9399(2005)131:11(1146).

[30] A. Mugadu, D.A. Hills, L. Limmer, An asymptotic approach to crack initiation in fretting fatigue of complete contacts, J. Mech. Phys. Solids. 50 (2002) 531–547. https://doi.org/10.1016/S0022-5096(01)00091-6.

[31] C.M. Churchman, D.A. Hills, General results for complete contacts subject to oscillatory shear, J. Mech. Phys. Solids. 54 (2006) 1186–1205. https://doi.org/10.1016/J.JMPS.2005.12.005.

[32] D.A. (David A. Hills, D. Nowell, A. Sackfield, Mechanics of elastic contacts, Butterworth-Heinemann, 1993.

[33] M. Ciavarella, D.A. Hills, G. Monno, The influence of rounded edges on indentation by a flat punch, Proc. Inst. Mech. Eng. Part C J. Mech. Eng. Sci. 212 (1998) 319–327. https://doi.org/10.1243/0954406981521259.

[34] R. Hojjati-Talemi, M. Abdel Wahab, J. De Pauw, P. De Baets, Prediction of fretting fatigue crack initiation and propagation lifetime for cylindrical contact configuration, Tribol. Int. 76 (2014) 73–91. https://doi.org/10.1016/J.TRIBOINT.2014.02.017.

[35] M. Sabsabi, E. Giner, F.J. Fuenmayor, Experimental fatigue testing of a fretting complete contact and numerical life correlation using X-FEM, Int. J. Fatigue. 33 (2011) 811–822. https://doi.org/10.1016/j.ijfatigue.2010.12.012.

[36] O. Jin, S. Mall, Influence of contact configuration on fretting fatigue behavior of

Ti-6Al-4V under independent pad displacement condition, Int. J. Fatigue. 24 (2002) 1243–1253. https://doi.org/10.1016/S0142-1123(02)00041-5.

[37] N. Gates, A. Fatemi, Multiaxial variable amplitude fatigue life analysis including notch effects, Int. J. Fatigue. 91 (2016) 337–351. https://doi.org/10.1016/J.IJFATIGUE.2015.12.011.

[38] C. Navarro, S. Muñoz, J. Domínguez, On the use of multiaxial fatigue criteria for fretting fatigue life assessment, Int. J. Fatigue. 30 (2008) 32–44. https://doi.org/10.1016/J.IJFATIGUE.2007.02.018.

[39] Y. Xue, D.L. McDowell, M.F. Horstemeyer, M.H. Dale, J.B. Jordon, Microstructure-based multistage fatigue modeling of aluminum alloy 7075-T651, Eng. Fract. Mech. 74 (2007) 2810–2823. https://doi.org/10.1016/J.ENGFRACMECH.2006.12.031.

[40] T. Webbe Kerekes, H. Lim, W.Y. Joe, G.J. Yun, Characterization of process–deformation/damage property relationship of fused deposition modeling (FDM) 3D-printed specimens, Addit. Manuf. 25 (2019) 532–544. https://doi.org/10.1016/j.addma.2018.11.008.